

Specific Absorption Rate (SAR) Electromagnetic (EM) Simulations in Adult and Child Tissues

Michel Alhilani¹, Seyed Reza Atefi², Lilla Zollei², Mohammad Mansouri², Filiz Yetisir¹, Michael H. Lev², P. Ellen Grant³, and Giorgio Bonmassar²

¹Newborn Medicine, Boston Children's Hospital/ Harvard Medical School, BOSTON, MA, United States

²Radiology, Massachusetts General Hospital/ Harvard Medical School, Boston, MA, United States,

³Newborn Medicine, Radiology, Boston Children's Hospital/ Harvard Medical School, Boston, MA, United States



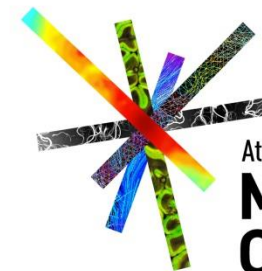
Athinoula A.
**Martinos
Center**
For Biomedical Imaging

 MASSACHUSETTS
GENERAL HOSPITAL

 HARVARD
MEDICAL SCHOOL

Introduction

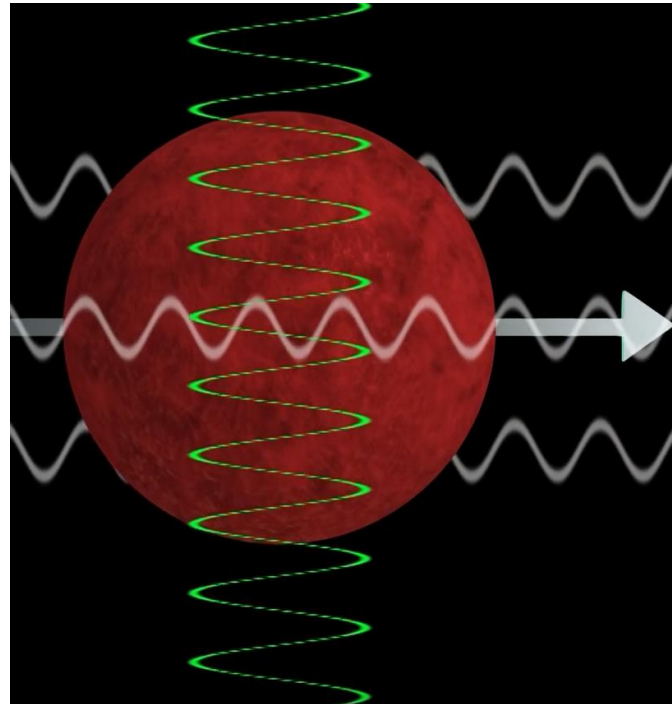
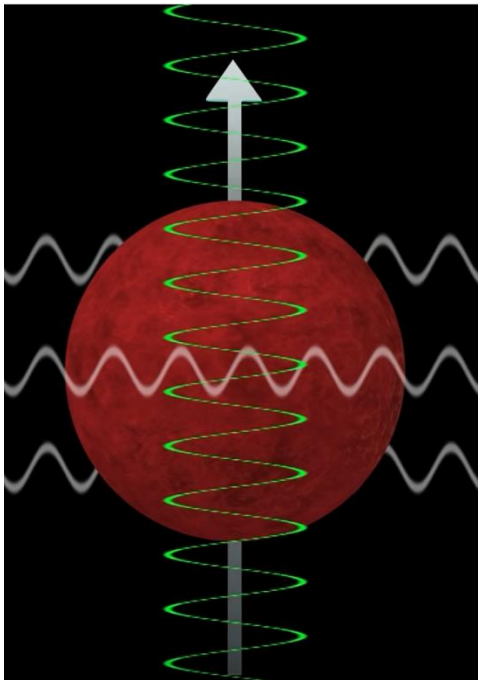
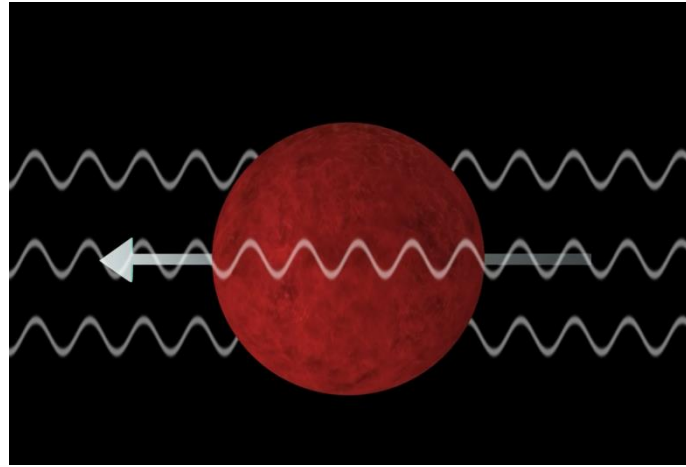
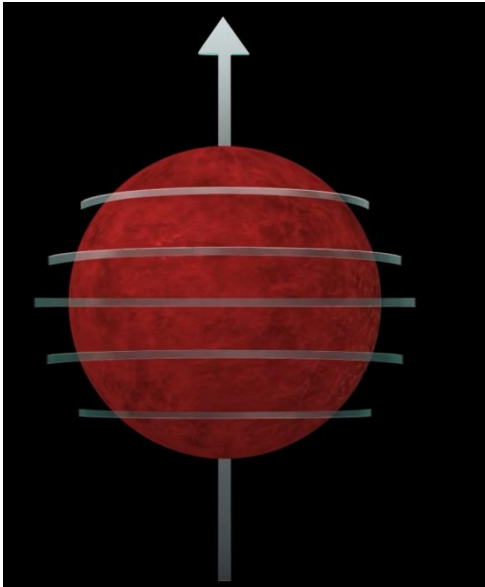
- Medical Images and devices for monitoring and diagnosis
- RX, MRI, CT, PET Imaging (Good Spatial Resolution)
- MRI



Athinoula A.
**Martinos
Center**
For Biomedical Imaging

MASSACHUSETTS
GENERAL HOSPITAL

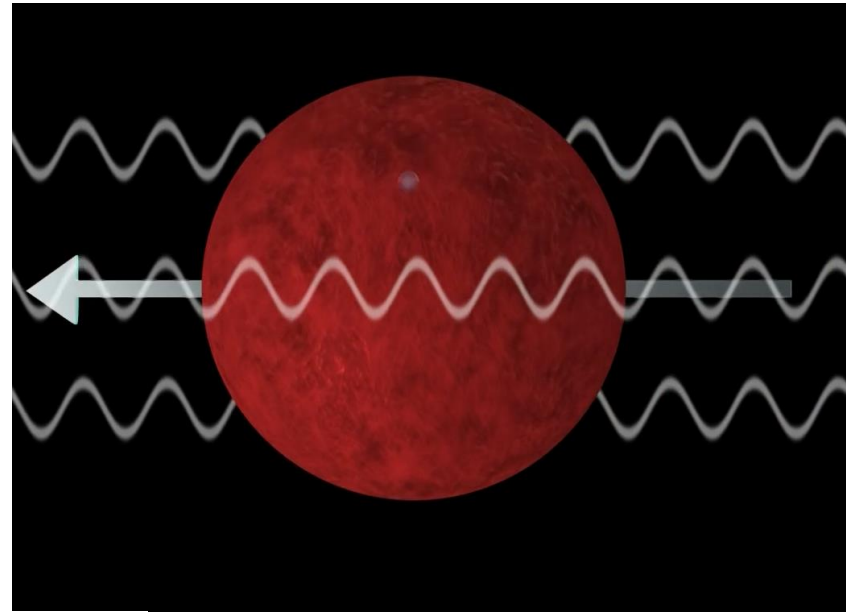
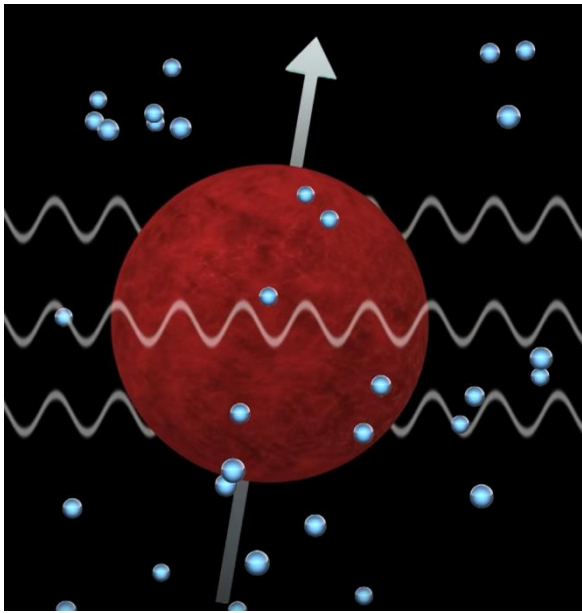
HARVARD
MEDICAL SCHOOL



Athinoula A.
Martinos
Center
For Biomedical Imaging

MASSACHUSETTS
GENERAL HOSPITAL

HARVARD
MEDICAL SCHOOL



MRI of a knee



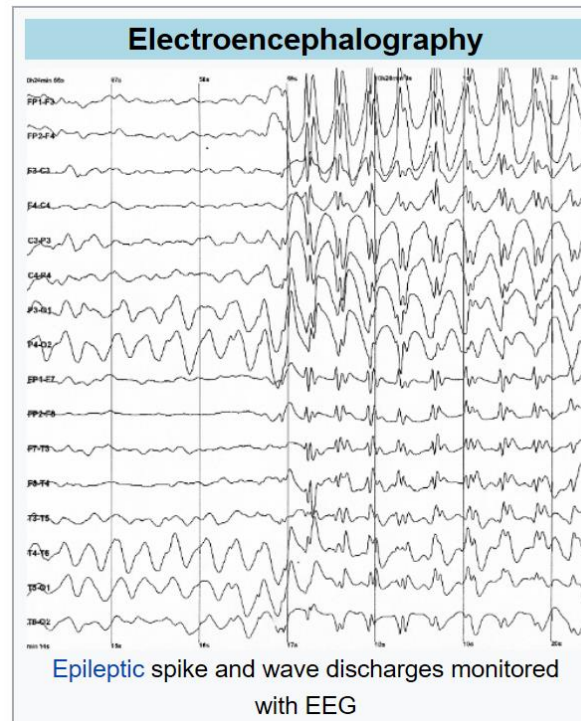
Athinoula A.
Martinos
Center
For Biomedical Imaging

MASSACHUSETTS
GENERAL HOSPITAL

HARVARD
MEDICAL SCHOOL

ELECTROENCEPHALOGRAPHY (EEG)

- Voltage fluctuations on ionic currents within the neurons
- EEG used to diagnose epilepsy, sleep disorders, depth of anesthesia, coma, encephalopathies, brain death, tumors and stroke.



Athinoula A.
**Martinos
Center**
For Biomedical Imaging



Advantages

- EEG has very high temporal resolution, on the order of milliseconds rather than seconds. EEG is commonly recorded at sampling rates between 250 and 2000 Hz in clinical and research settings, but modern EEG data collection systems are capable of recording at sampling rates above 20,000 Hz if desired



Athinoula A.
**Martinos
Center**
For Biomedical Imaging



Disadvantages

- Low spatial resolution on the scalp
- EEG poorly measures neural activity that occurs below the upper layers of the brain (the cortex).
- Cannot identify specific locations in the brain at which various neurotransmitters, drugs, etc. can be found.
- Signal-to-noise ratio is poor, so sophisticated data analysis and relatively large numbers of subjects are needed to extract useful information from EEG.



Athinoula A.
**Martinos
Center**
For Biomedical Imaging



What if



+



Laufs, H; et al., (2003). "EEG-correlated fMRI of human alpha activity". *NeuroImage*. **19** (4): 1463–76
Difrancesco, Mark W.; et al. (2008). "Simultaneous EEG/Functional Magnetic Resonance Imaging at 4 Tesla: Correlates of Brain Activity to Spontaneous Alpha Rhythm During Relaxation"



Athinoula A.
**Martinos
Center**
For Biomedical Imaging



What if ... issues

- The radiofrequency (RF) power from MRI deposited in the tissues can cause excess heat in the tissue and causes tissue burns.
- A measure of this heating effect is known as specific absorption rate (SAR), defined as the power absorbed per mass of tissue. Its measure is units of watt per kilogram (W/kg). Usually, SAR is averaged over either the whole body or a small sample volume (typically 1 g or 10 g of tissue). SAR can be measured as an average value in the whole head or in the whole body



Athinoula A.
**Martinos
Center**
For Biomedical Imaging



What if ... issues

- In 2014, the FDA regulated the maximum whole-body SAR values in various parts of the human body per unit time. These SAR limits stipulate that the maximum whole-body SAR is 4 W/kg averaged over 15 minutes in the whole body, and 3.2 W/kg averaged over 10 minutes in the head
- However, the 2014 standard does not provide any limits to the 10g-SAR which is relevant for heating



Athinoula A.
**Martinos
Center**
For Biomedical Imaging



Implants and SAR

- Metallic implants or medical devices can interact with MRI radiofrequency field resulting in elevated SAR and tissue burns as well as image artifact.
- Simultaneous EEG-fMRI is one case in which metallic traces of the EEG net can interact with MRI RF field resulting in elevated SAR and Image artifacts



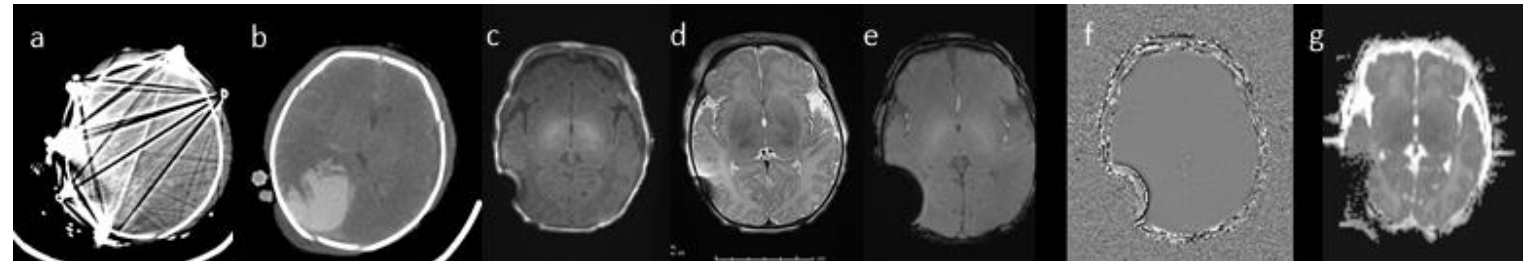
Athinoula A.
**Martinos
Center**
For Biomedical Imaging

 MASSACHUSETTS
GENERAL HOSPITAL

 HARVARD
MEDICAL SCHOOL

EEG leads artifact on MRI and CT

The so-called “MRI compatible” EEG-electrodes still produce visible CT/MRI image artifacts.



(a-b) Two days old male with Hypoxic Ischemic Encephalopathy (HIE) and complex congenital heart disease on extracorporeal membrane oxygenation (ECMO) to provide heart and lung support. EEG leads are in place as part of routine HIE monitoring. Emergent CT ordered because of sudden onset of status epilepticus. a) CT with EEG soft tissue algorithm. b) CT 6 hours later without EEG revealed a hematoma originally missed due to artifacts on the prior CT. **(c-e)** MRI from a 3-day old term neonate with severe perinatal depression requiring resuscitation at birth after a STAT C-section thus needing EEG monitoring: c) axial reformation of magnetization-prepared rapid gradient-echo (MP-RAGE) d) Turbo Spin Echo (TSE) e) Susceptibility Weighted Imaging (SWI) f) SWI phase map and g) Apparent diffusion coefficient (ADC) map. Artifacts from EEG leads limit ability to detect brain abnormalities.

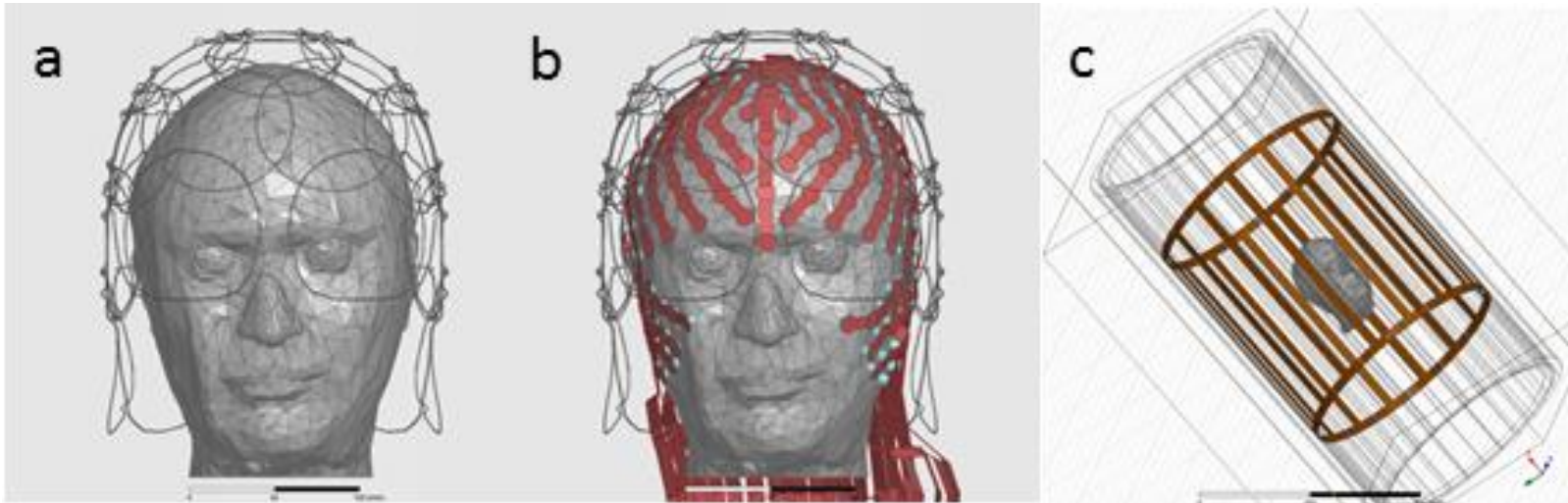


Athinoula A.
**Martinos
Center**
For Biomedical Imaging

MASSACHUSETTS
GENERAL HOSPITAL

HARVARD
MEDICAL SCHOOL

Numerical Modeling and simulation for MRI Heating Safety Evaluation of Implants



- Requires Anatomically accurate modeling of tissues
- Implants
- MRI Coils

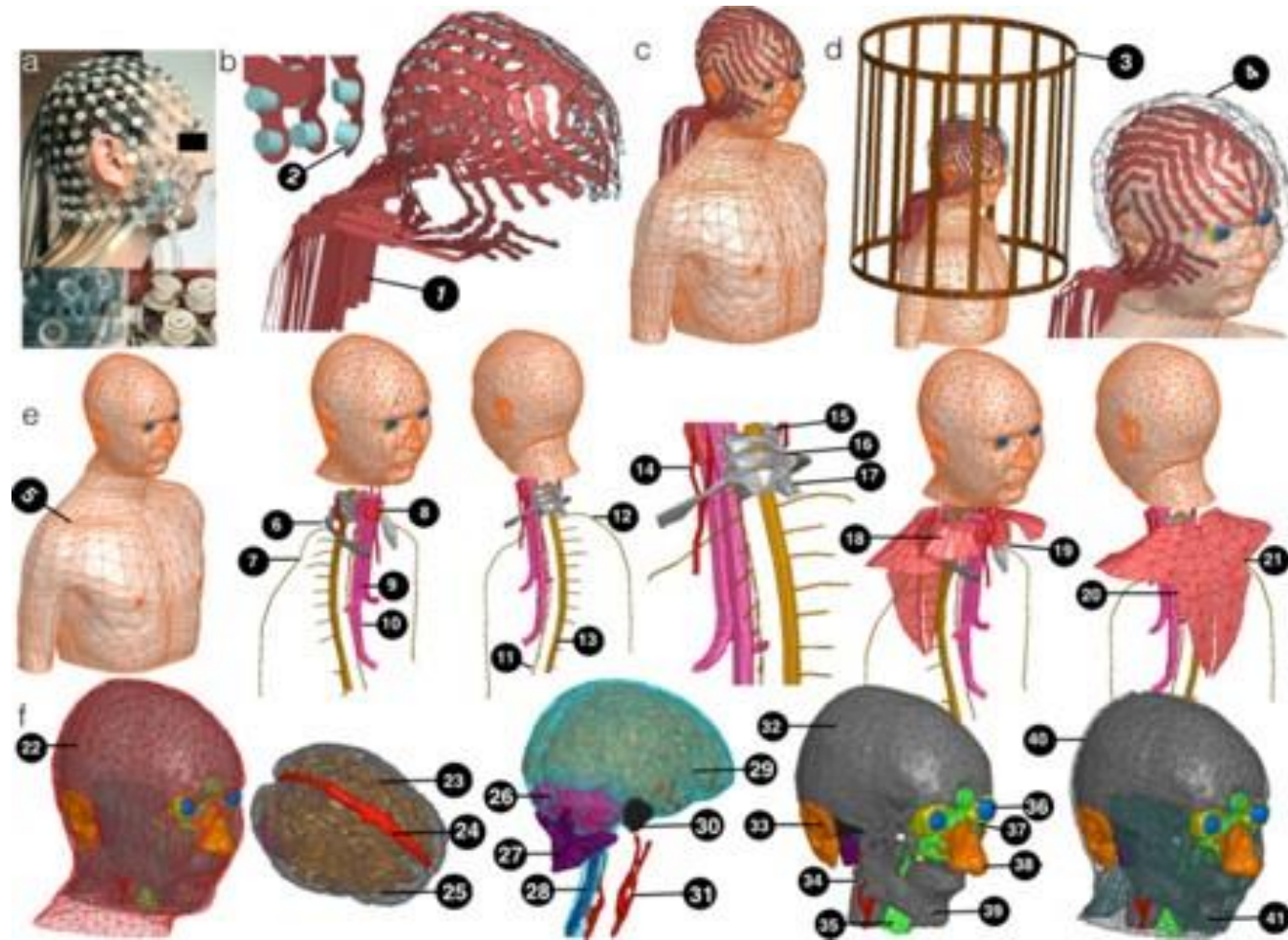


Athinoula A.
**Martinos
Center**
For Biomedical Imaging



Accurate Models for Simulation

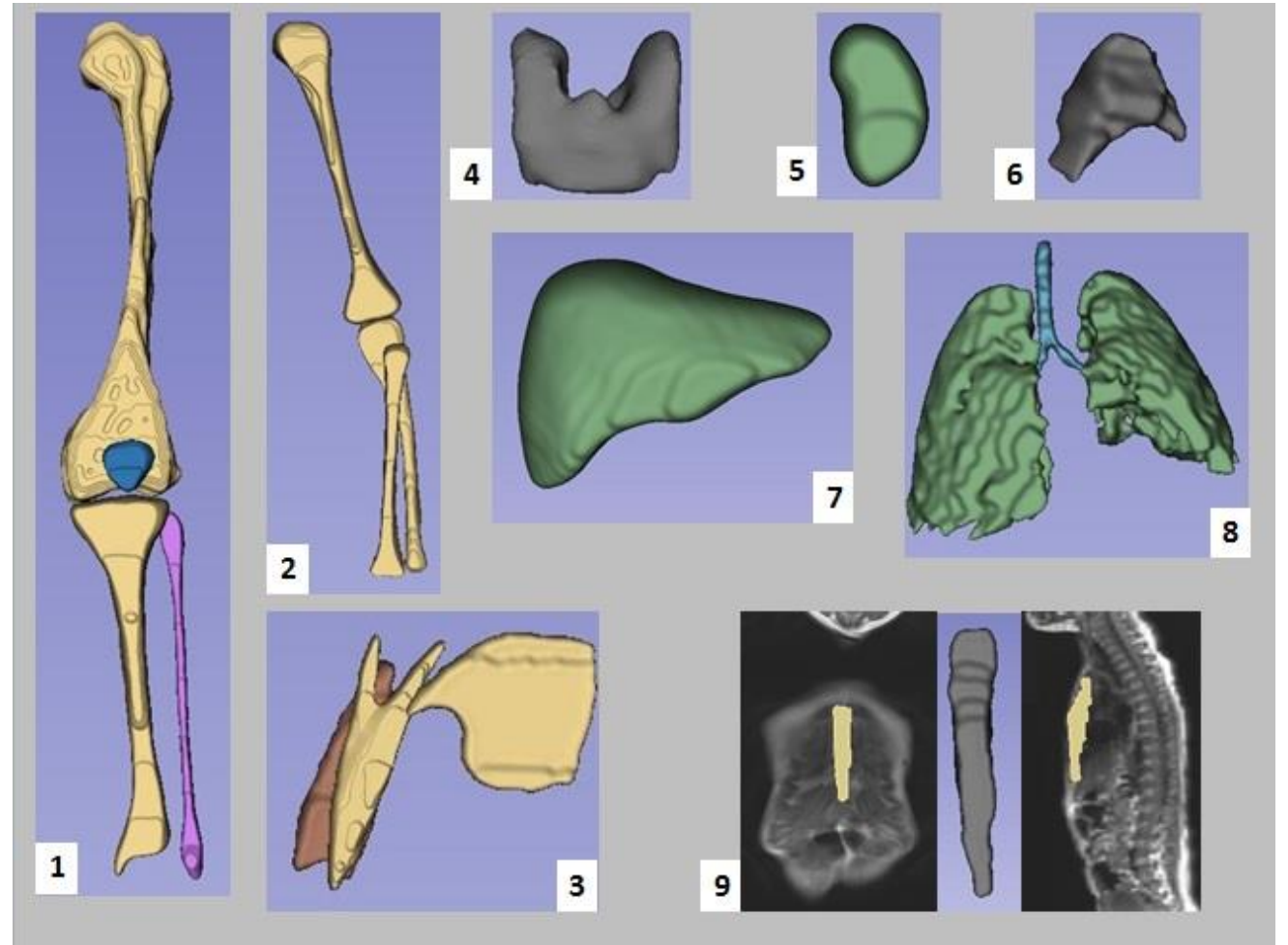
- (a) 256-channel dEEG cap with lead wires printed with conductive ink (InkNet) [1] (b) CAD model of the Ink-Cap showing 1) leads and 2) pedestals (c) anatomical model of 37 year-old male subject wearing the dEEG cap model (d) loaded in MRI 3) transmit and 4) receive coils; (e) body model and anatomical structures in the torso including 5) muscle, 6) right-side ribs, 7) right-side nerves, 8) larynx, 9) trachea, 10) oesophagus, 11) spinal cord, 12) left-side nerves, 13) brainstem, 14) carotid arteries, 15) C4 bone, 16) C5 bone, 17) T1 bone, 18) muscle plat right, 19) muscle plat left, 20) left trapezius muscle, 21) right trapezius muscle, (f) head model including 22) epidermis/dermis, 23) white matter, 24) blood, 25) grey matter, 26) cerebellum, 27) adipose 28) spinal cord nerve, 29) Cerebrospinal fluid (CSF), 30) mastoid bone, 31) carotid arteries, 32) skull, 33) ears, 34) vertebral column, 35) air sinus, 36) eye with lens and humor, 37) orbital fat, 38) nose, 39) facial bone, 40) muscle, 41) subcutaneous tissue including muscle cartilage and



Athinoula A.
Martinos Center
 For Biomedical Imaging



Segmentation with 3D Slicer/RETOMO

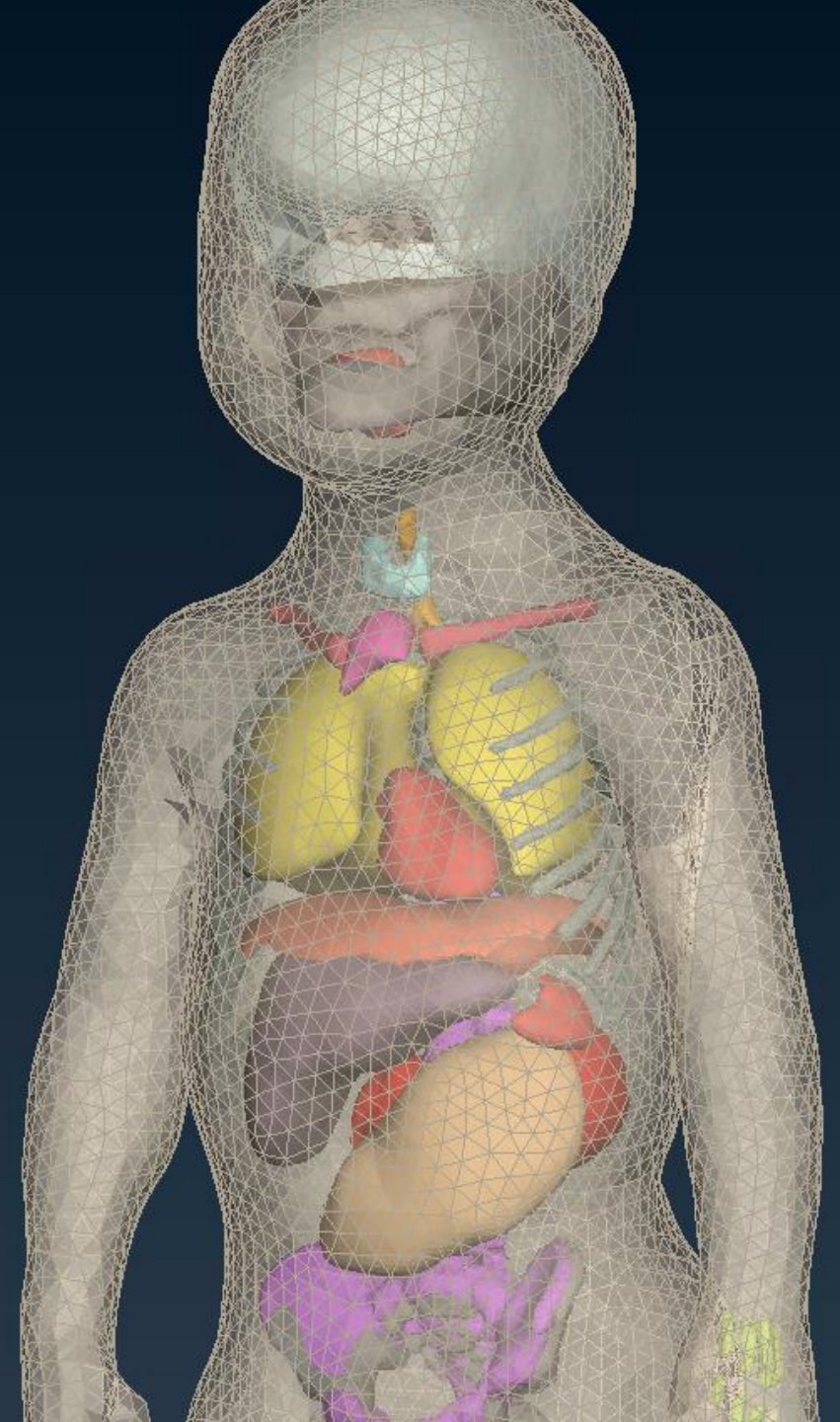


Athinoula A.
**Martinos
Center**
For Biomedical Imaging



Pediatric Modeling for MRI Safety Studies

Cleaning the mesh using ANSA from BETA CAE



ANSA v19.1.2 64-bit (C:/Users/milton/Desktop/REZA_Harvard/Second_Model/Firstattemptvolumemesh.ansa)

File Tools Utilities Lists Assembly Plugins Windows Help

Search Functions and Filters

Database

Name	Number
ANSAPART	9
EDGE	
<input checked="" type="checkbox"/> ELEMENT	5600965
<input type="checkbox"/> GEOMETRY	3
<input type="checkbox"/> MATERIAL	6
<input type="checkbox"/> NODE	905517
<input type="checkbox"/> PROPERTY	6
SOLIDFACET	
<input type="checkbox"/> STEP	1
<input checked="" type="checkbox"/> VOLUME	2

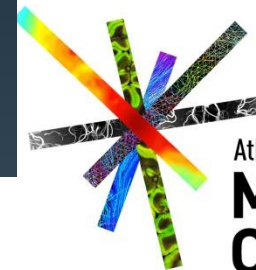
Firstattemptvolumemesh.ansa, Current Part: Untitled

```

Shell
quads : 0
trias : 257098
total : 257098

Volume
tetras : 1532574
total : 1532574

```



Athinoula A.
**Martinos
Center**
For Biomedical Imaging

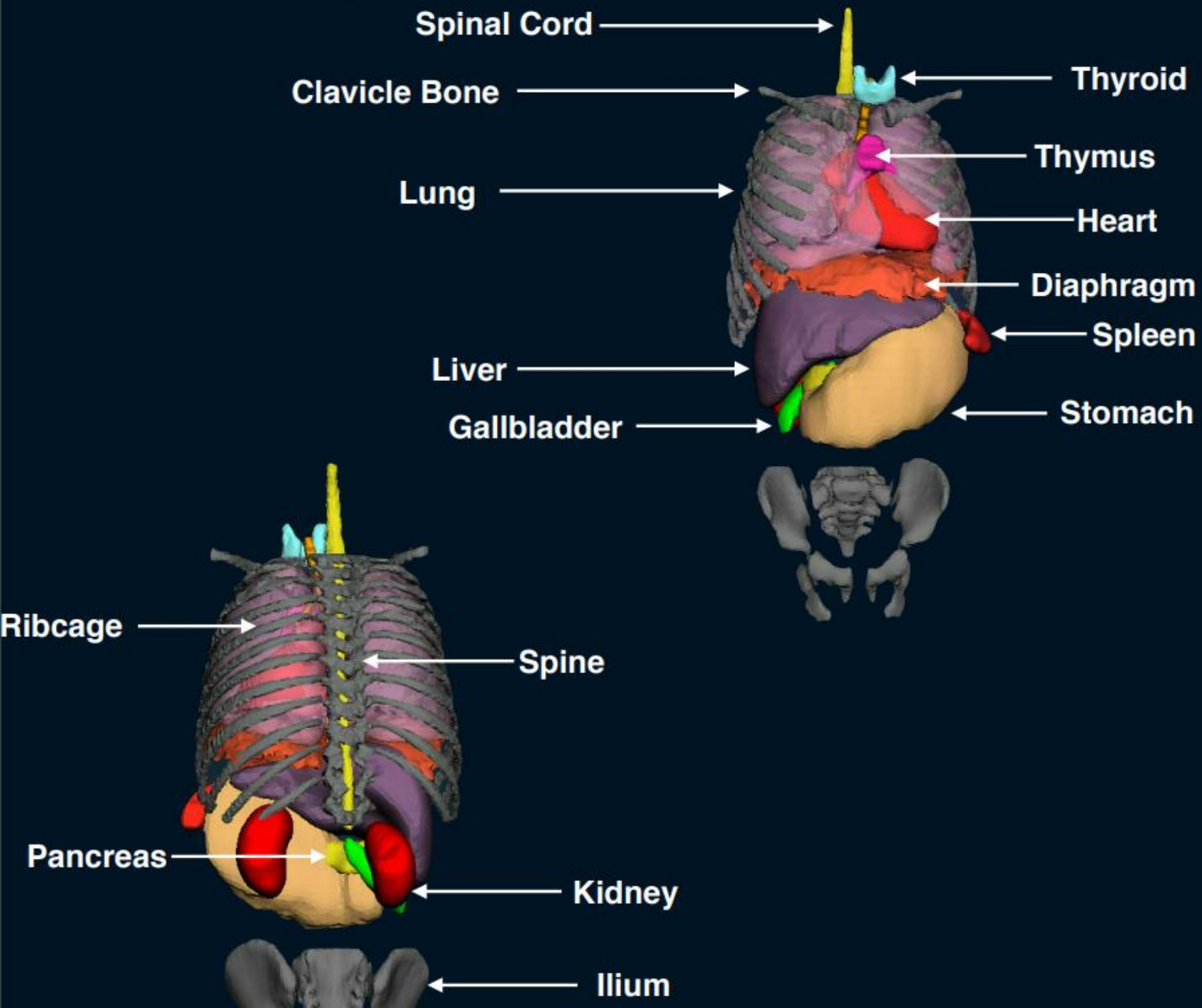
MASSACHUSETTS
GENERAL HOSPITAL

HARVARD
MEDICAL SCHOOL



ANSA from BETA CAE will allow Surface
Model Mesh Preprocessing for Simulations
with FEM Packages

ABI Lab Segmentation



Segmentations
cleaned in ANSA



Athinoula A.
**Martinos
Center**
For Biomedical Imaging

MASSACHUSETTS
GENERAL HOSPITAL

HARVARD
MEDICAL SCHOOL

Methods and Simulation Parameters

- MRI imaging was performed on a 3T scanner (TIM TRIO, Siemens AG, Erlangen, Germany). The sequences included whole body coronal T1-weighted and MPRAGE of the brain.
- Manual segmentation was done using 3D Slicer [1]
- For the whole skin surface, MedianImageFilter was used for noise reduction, then a 3D surface model was created from grayscale data
- STL meshes from 3D Slicer were enhanced by removing intersecting elements, filling gaps, removing noise, mesh size, quality using ANSA



Athinoula A.
**Martinos
Center**
For Biomedical Imaging



Methods and Simulation Parameters

- FEM was used to simulate the SAR in the single tissue child and adult model at 3T MRI.
- The RF transmit coil dimensions were according to [2], and the coil was tuned as described in [2]. Tuning capacitance of 13.5 pF was used until the unloaded coil system was tuned at 128 MHz.
- The coil input ports were sinusoidal voltage of identical magnitude and 90° phase difference to generate quadrature excitation. Input excitations were on the superior end ring of the coil at 45° and 135° angles and defined as input ports.



Athinoula A.
**Martinos
Center**
For Biomedical Imaging



Methods and Simulation Parameters

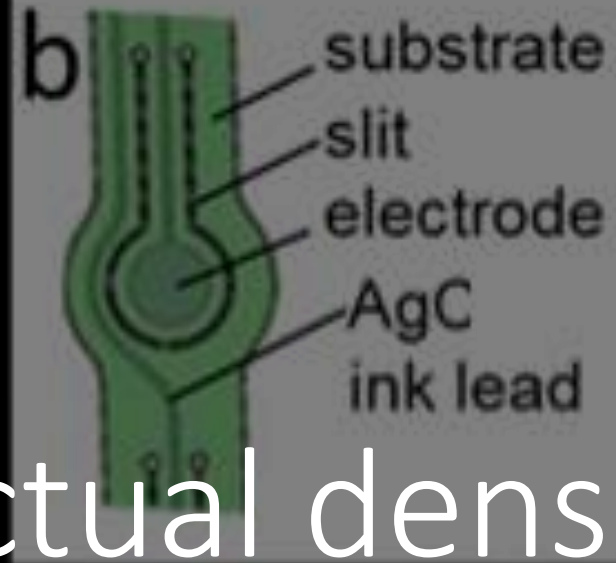
- A circuit solution comprised of a set of 32 voltage amplitude and phase offset inputs were computed and included in the high-frequency structural simulator (HFSS) model to scale the 3D field solution to the tuned coil condition, using a 13.5-pF tuning capacitance. The input voltage of the coil input ports was then adjusted to 144 V in the circuit simulator to deliver of 4 W/kg whole body SAR [3].



Athinoula A.
**Martinos
Center**
For Biomedical Imaging



a



Modeling the actual dense array EEG net

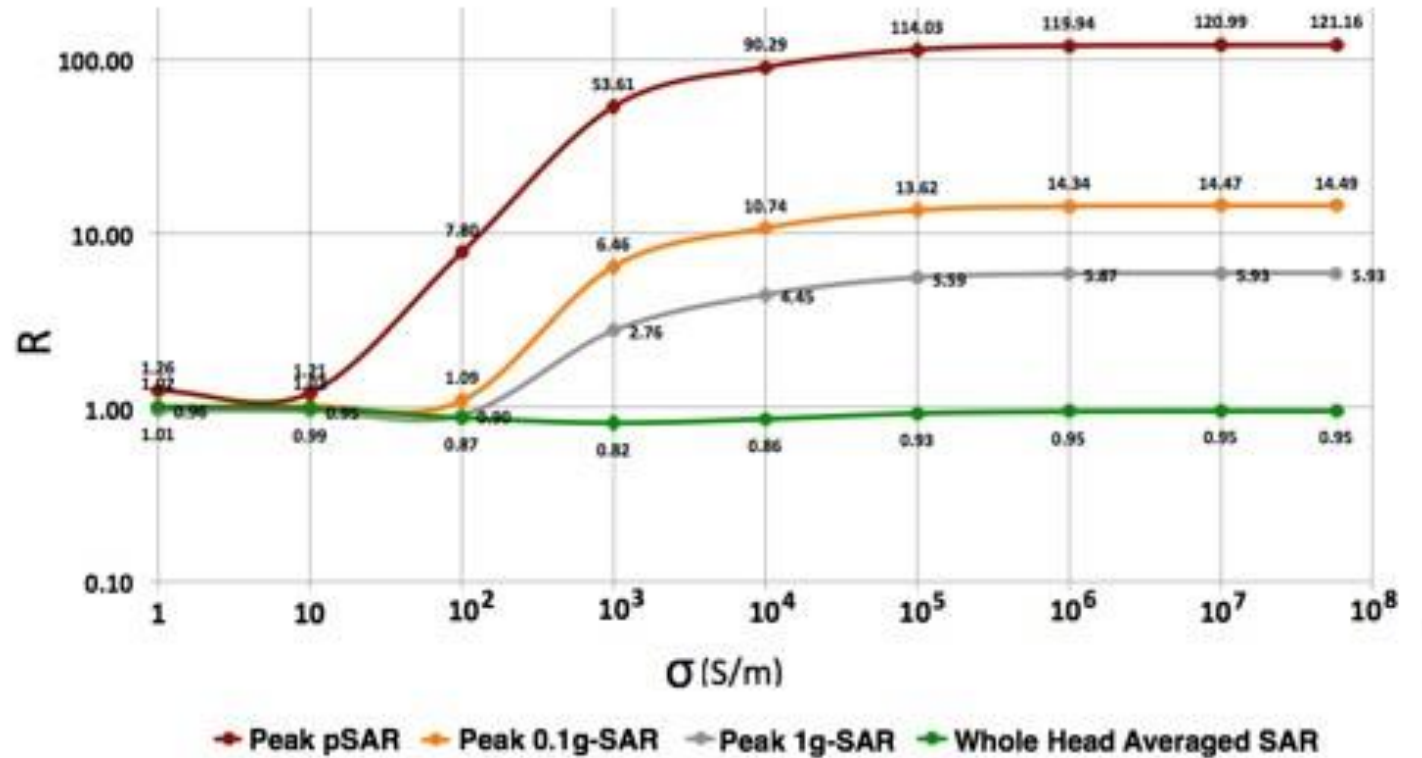
Leads made of conductive INK instead of traditional copper wires



Test New Design Options

- Highly conductive leads like copper used in traditional EEG nets can cause greater SAR less conductive leads
- Using numerical simulations one can easily quantify the effect of different lead conductivities on SAR averaged in different tissue mass
- Conductive ink with conductivities in the range 10 S/m are a good option

$$R = \frac{SAR_{\text{EEG Net}}}{SAR_{\text{No-Net}}}$$



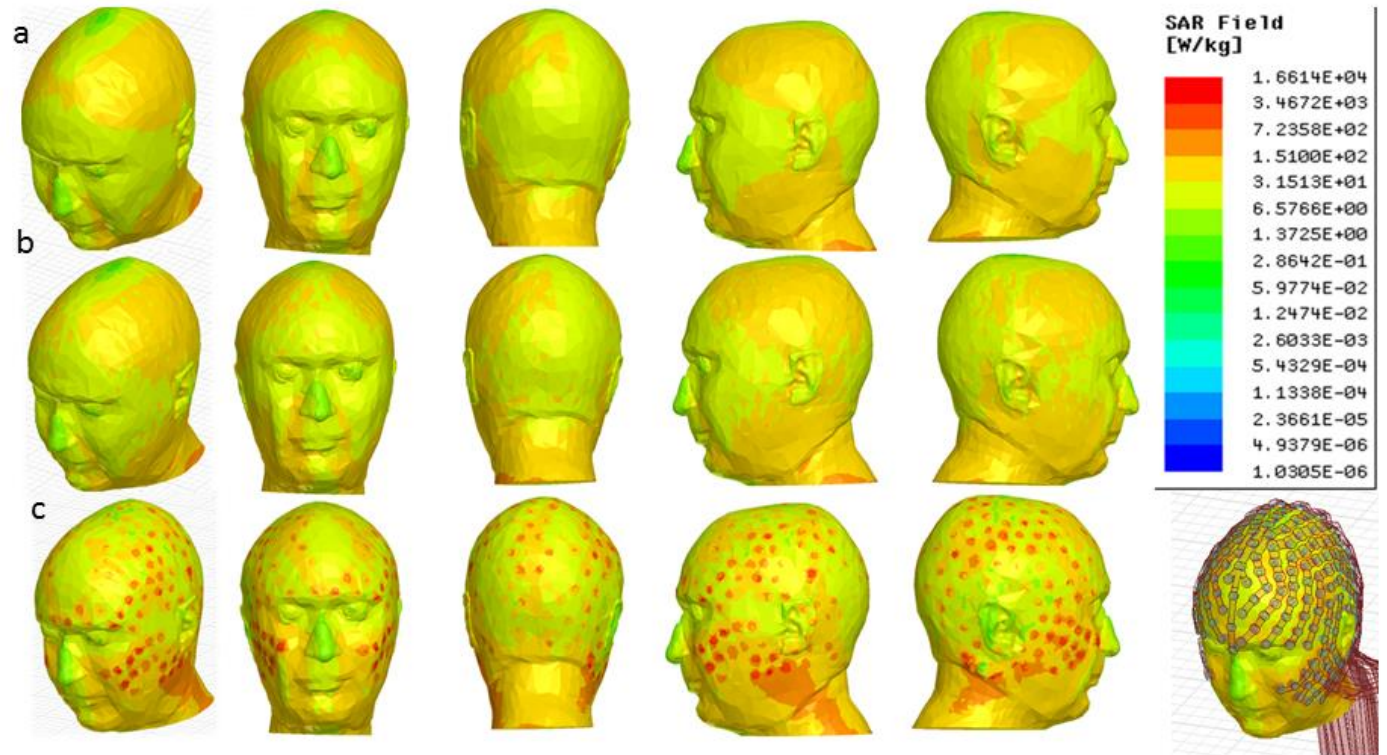
Values of R for nine EEG lead conductivity σ for peak of pSAR, peak of 0.1g-SAR, peak 1g SAR and SAR averaged in the whole head.



Athinoula A.
Martinos Center
For Biomedical Imaging

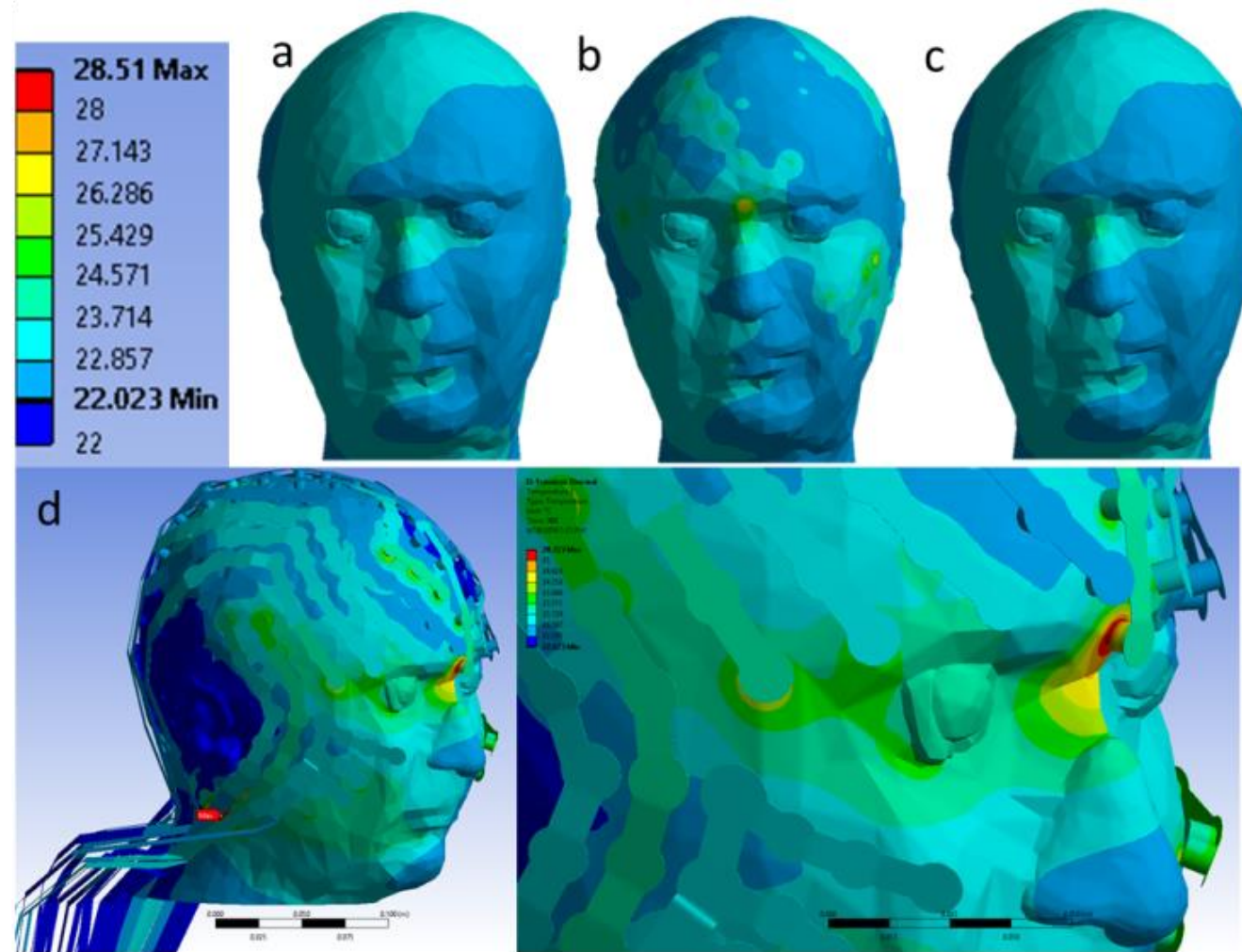
SAR evaluation in the adult model

3 Tesla 1g averaged SAR (W/kg) of the head model wearing: a) no Net, b) InkNet and c) a copper based Net (CopperNet). The 1g-averaged SAR of InkNet is similar to the gold standard of no Net while CopperNet shows local SAR hot spots (red dots), which are in the precise location where the EEG electrodes are located (right).



Thermal simulations from SAR fields

Simulated temperature changes in a phantom (°C) model wearing a) NoNet, b) CopperNet, c) InkNet, d) NoNet, which showed the temperature hot spot in the nasion location near the eyes.

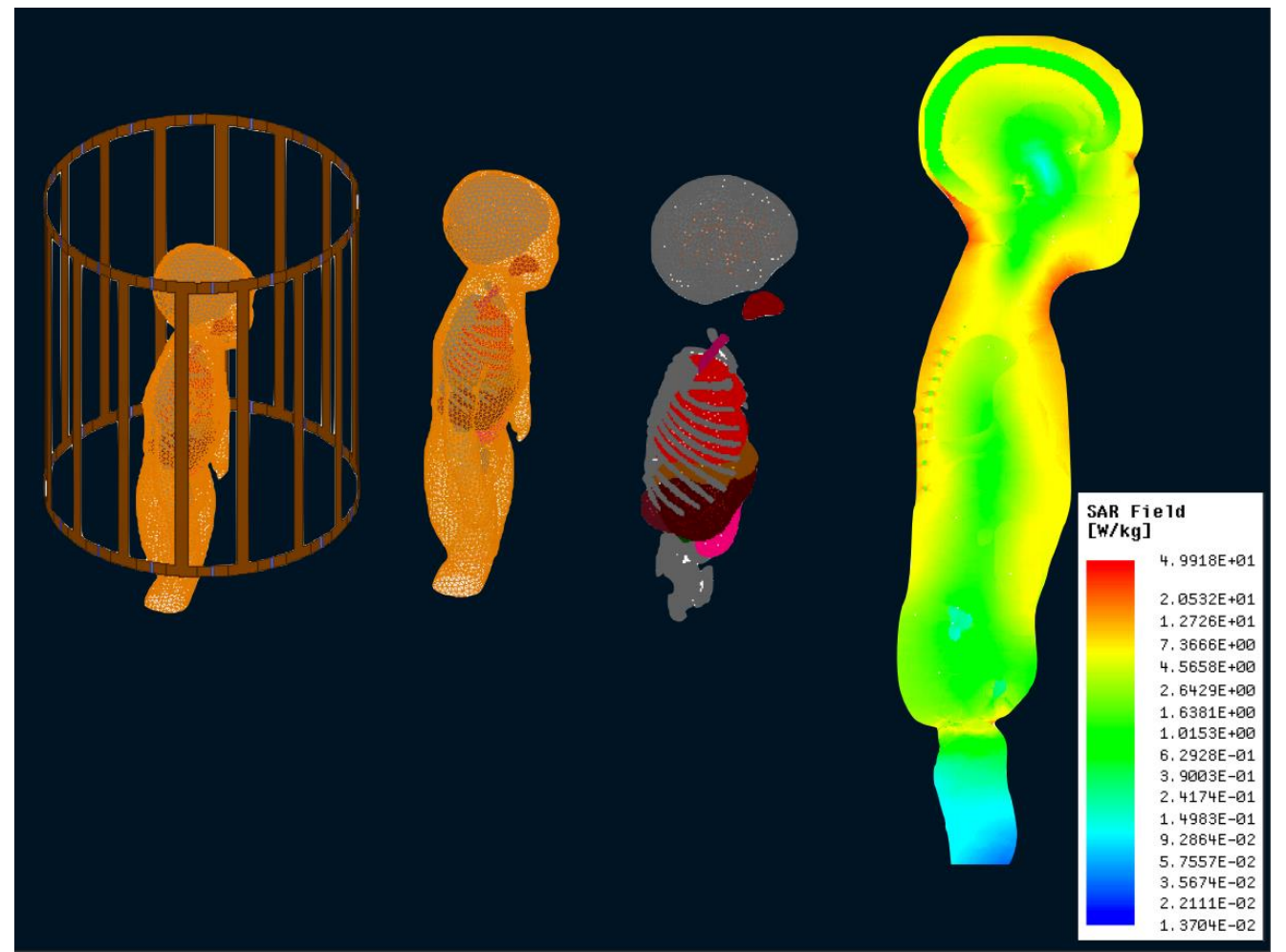


Athinoula A.
Martinos Center
For Biomedical Imaging



Feasibility Simulations

- Feasibility of SAR Evaluation in the Segmented and cleaned Pediatric Model



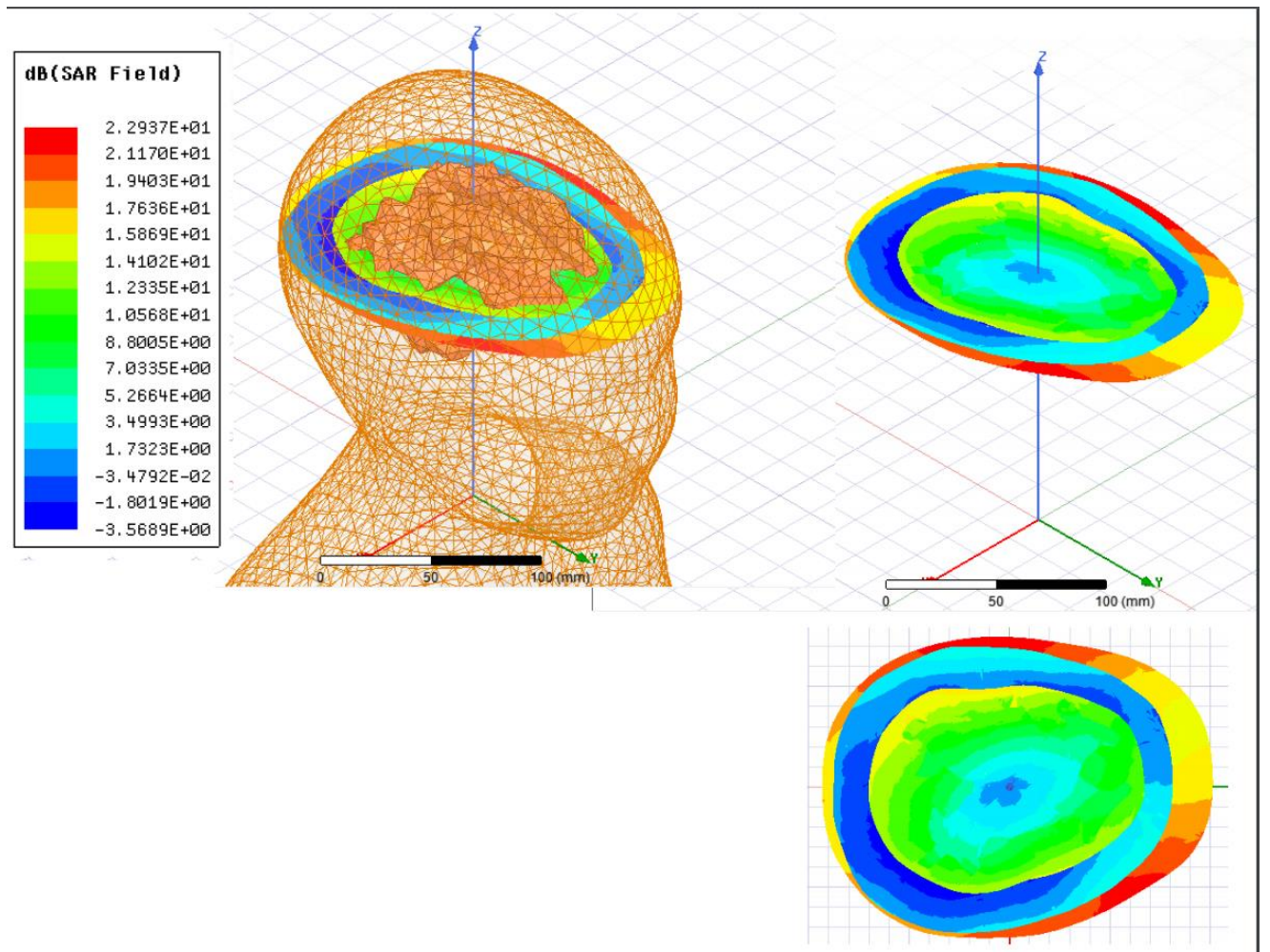
Athinoula A.
**Martinos
Center**
For Biomedical Imaging

MASSACHUSETTS
GENERAL HOSPITAL

HARVARD
MEDICAL SCHOOL

Feasibility Simulations

- Feasibility of SAR Evaluation in the Segmented and cleaned Pediatric Model

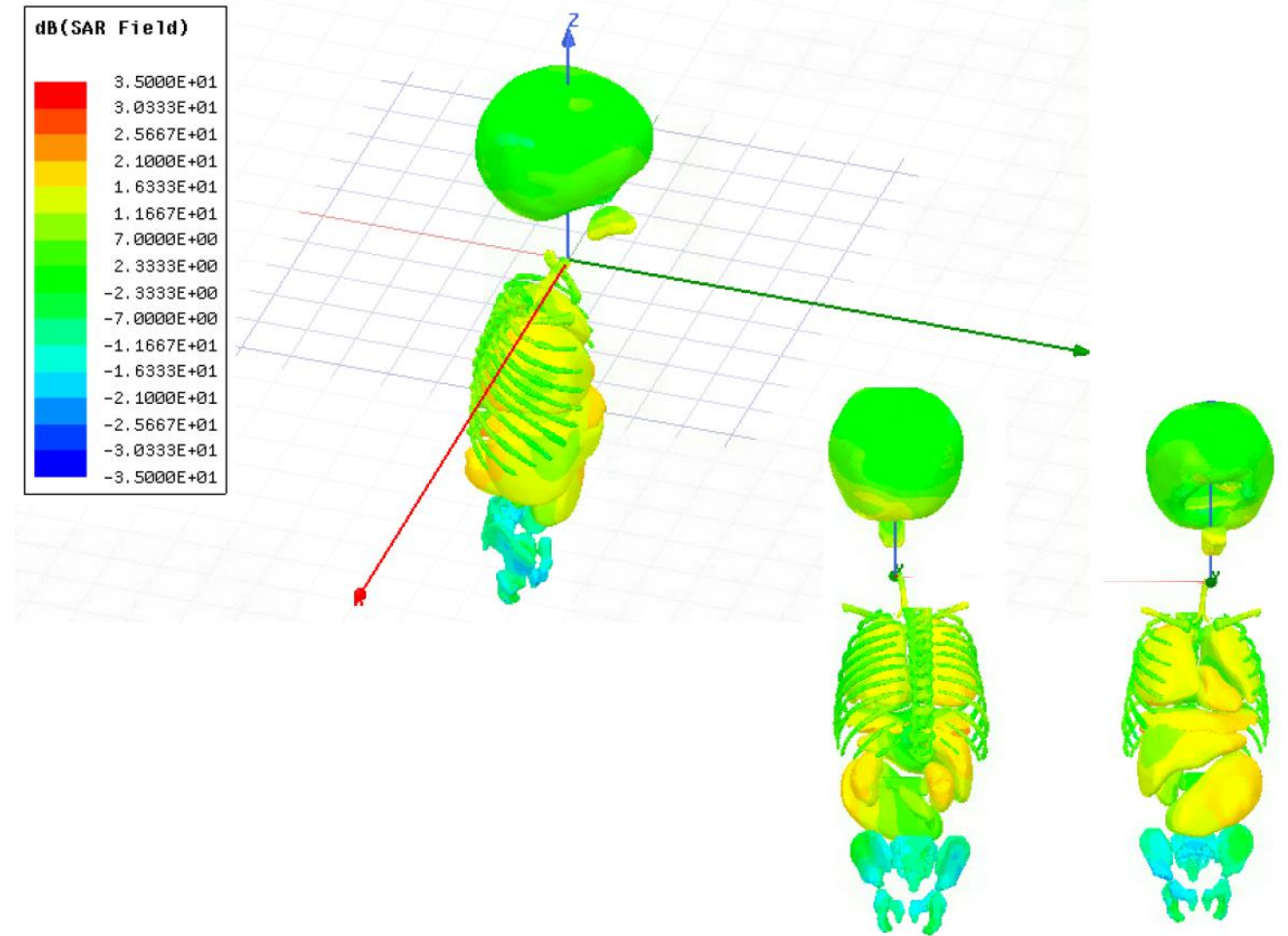


Athinoula A.
Martinos Center
For Biomedical Imaging



Feasibility Simulations

- Feasibility of SAR Evaluation in the Segmented and cleaned Pediatric Model



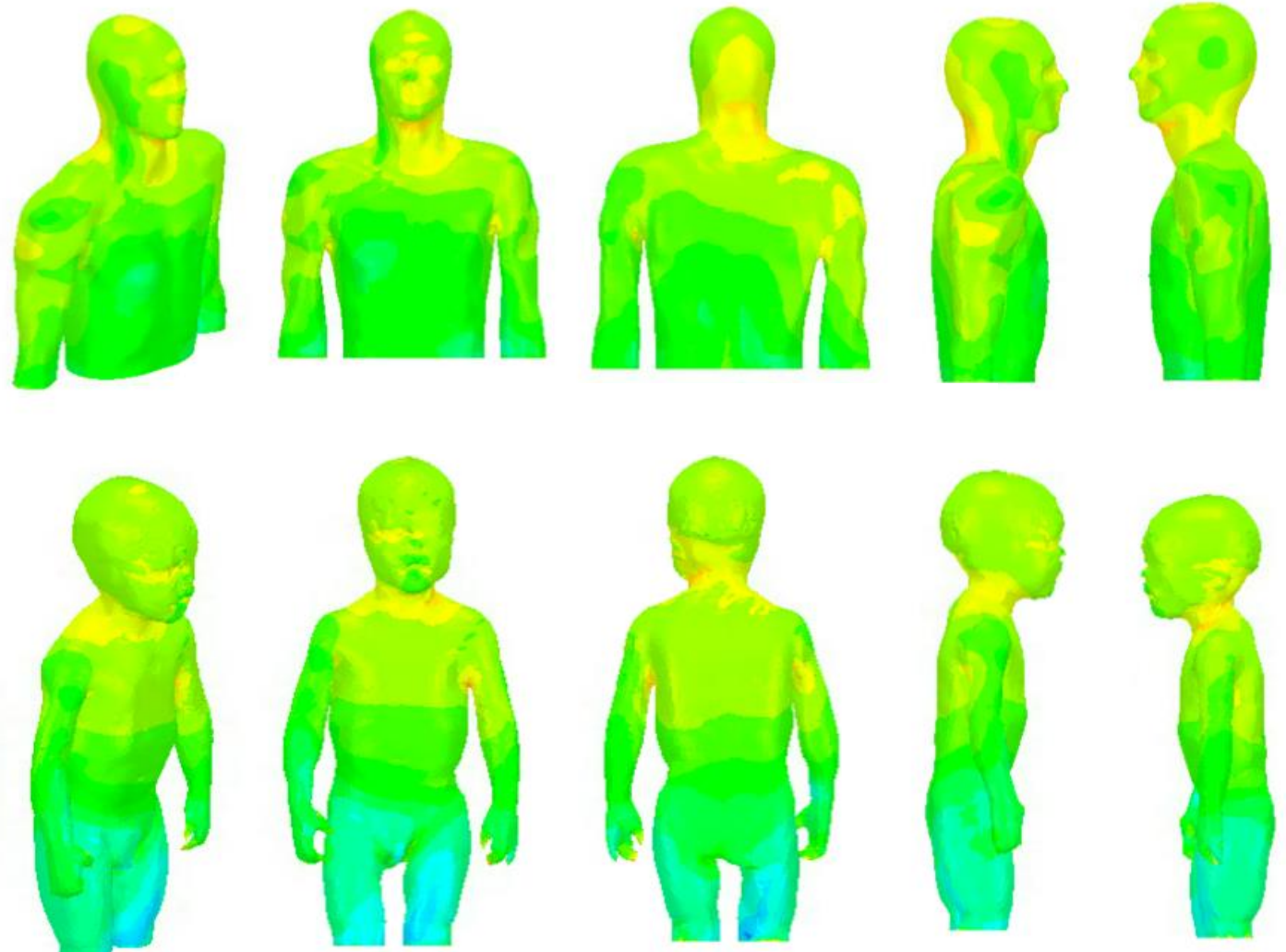
Athinoula A.
Martinos Center
For Biomedical Imaging

MASSACHUSETTS
GENERAL HOSPITAL

HARVARD
MEDICAL SCHOOL

Comparison of SAR in the adult and pediatric models

- The whole body averaged SAR was 4 W/kg for both the adult and child models
- The simulations showed that the adult local SAR peak was 2,054W/kg, while the child local SAR peak was 334W/kg or approximately 6x smaller.
- In both models, the local SAR peaks were located in the neck and armpits.
- 10g SAR peak in the adult model was 43.6 W/kg, while the child model had 31.88 or a 1.4x smaller peak.



Athinoula A.
**Martinos
Center**
For Biomedical Imaging

MASSACHUSETTS
GENERAL HOSPITAL

HARVARD
MEDICAL SCHOOL

References

- [1] Fedorov A., Beichel R., Kalpathy-Cramer J., Finet J., Fillion-Robin J-C., Pujol S., Bauer C., Jennings D., Fennessy F., Sonka M., Buatti J., Aylward S.R., Miller J.V., Pieper S., Kikinis R. 3D Slicer as an Image Computing Platform for the Quantitative Imaging Network. *Magnetic Resonance Imaging*. 2012 Nov;30(9):1323-41.
- [2] G. Bonmassar, P. Serano, and L. M. Angelone, "Specific absorption rate in a standard phantom containing a deep brain stimulation lead at 3 Tesla MRI," in *Proc. 6th Int. IEEE/EMBS Conf. Neural Eng.*, 2013, pp. 747–750.
- [3] *Medical Electrical Equipment—Part 2-33: Particular Requirements for the Basic Safety and Essential Performance of Magnetic Resonance Equipment for Medical Diagnosis*, TC 62/SC 62B, 2015.



Athinoula A.
**Martinos
Center**
For Biomedical Imaging



Acknowledgements

- This work was funded by NIH/NIBIB grant R01EB024343

